A&A 454, 595–607 (2006)
DOI: 10.1051/0004-6361:20054350

Astronomy & Astrophysics

X-ray emission from T Tauri stars in the Lupus 3 star-forming region⋆,⋆⋆

P. Gondoin

European Space Agency, ESTEC – Postbus 299, 2200 AG Noordwijk, The Netherlands
e-mail: pgondoin@rssd.esa.int

Received 13 October 2005 / Accepted 15 March 2006

ABSTRACT

Aims. In this paper, I present analysis results of an *XMM − Newton* observation of the Lupus 3 region that contains a high proportion of young low mass ($M < 0.3\ M_{\odot}$) T Tauri stars in the Lupus star-forming complex.
Methods. The detection of X-ray sources in 0.5 to 4.5 keV images of the Lupus 3 core was performed using the standard source detection method of the *XMM − Newton* Science Analysis Software. The detected sources were correlated with a list of Herbig-Haro objects and H_{α} emission stars that contains mainly classical T Tauri stars, with a catalogue of weak-line T Tauri Stars and with a recent list of new low-mass members of the Lupus 3 dark cloud found in a visible-light spectroscopic survey at the center of the Lupus 3 star-forming core. The light curves and spectra of the brightest X-ray sources with known T Tauri star counterparts were analysed.
Results. One hundred and two X-ray sources were detected in the 30′ diameter field-of-view of the EPIC cameras, of which 25 have visible or near-IR counterparts that are known as pre-main sequence stars. Their X-ray luminosity ranges from 3×10^{28} to 3×10^{30} erg s^{-1}. Two of these objects with mass estimates lower than 0.075 $M_{\odot}$ have an X-ray luminosity of about 4–7 $\times 10^{28}$ erg s^{-1}, comparable with that of flaring young brown dwarfs. A linear correlation is found between the X-ray luminosity and the mass or volume of the stars that is qualitatively expected from some models of distributed turbulent dynamos. The EPIC spectra of the X-ray brightest sources can be fitted using optically thin plasma emission models with two components at temperatures in the ranges 3–9 $\times 10^6$ K and 1–50 $\times 10^7$ K, respectively. The large emission measure of hot plasma may be caused by disruptions of magnetic fields associated with an intense flaring activity, while the X-ray emission from the "cool" plasma components may result from solar-type active regions. The emission measures of the plasma components are of the order of 10^{52} cm^{-3}, typical of the values expected from coronal plasmas in T Tauri stars, post-T Tauri stars, and active late-type dwarfs in close binary systems. One property of the X-ray brightest stars in Lupus 3 that seems common among pre-main sequence stars is the low abundance of Fe.

Key words. stars: activity – stars: atmospheres – stars: coronae – stars: evolution – stars: low-mass, brown dwarfs - stars: late-type

1. Introduction

The Lupus star-forming complex is one of the belts of low mass star-forming regions within 200 pc from the Sun, together with those of Chameleon, ρ Ophiuci, R Coronae Australis, and Taurus. Its population of T Tauri-stars is concentrated in four small subgroups (Lupus 1-4) that are distinct, loosely connected entities scattered over a large area of the sky and approximately at the same distance (Hughes et al. 1993). A survey of the pre-main sequence population associated with the Lupus clouds has been carried out by Schwartz (1977), who extended the list of Hα-emitting members previously identified by Henize (1954) and The (1962). A detailed spectroscopy study of many of the members identified in Schwartz's work is reported by Hughes et al. (1994). These studies were performed on a survey sample of "Classical" T Tauri Stars (CTTS), and not on the total population of pre-main sequence stars (PMS). The known PMS population in Lupus was significantly increased when "Weak-line" T Tauri Stars (WTTS) were detected by *ROSAT*. Identification of *ROSAT* sources in the area of the Lupus star-forming region has led to the discovery of 136 new T Tauri stars (Krautter et al. 1997; Wichmann et al. 1997a), of which the large majority are WTTS. These stars are most easily detected and identified as WTTS in the X-ray band. Due to their lack of strong emission lines in the optical spectral range, most of the WTTS are not detected by optical objective prism surveys like those carried out by The (1962) and Schwartz (1977). The X-ray survey of Krautter et al. (1997) excludes all X-ray sources without a stellar counterpart of R magnitude $m_R \leq 15$, which converts to $m_V \leq 16$ for an M2V star. The survey of Wichmann et al. (1997a) was limited to *ROSAT* All Sky Survey (RASS) sources with GSC counterparts that are rarely fainter than $m_V \approx 14$. For comparison, some of the H_{α} survey sources identified by Schwartz (1977) reach a V magnitude $m_V \approx 17.5$ (Hughes et al. 1994).

Recently, special attention was paid to the Lupus 3 cloud, the one containing the richest stellar aggregate. Nakajima et al. (2000) identified new faint, moderately obscured members with estimated masses near the sub-stellar limit by means of near-infrared imaging. This confirmed the unusual mass spectrum of stars in this region which exhibits a higher proportion of very

⋆ Based on observations obtained with XMM-Newton, an ESA science mission with instruments and contributions directly funded by ESA Member States and NASA.

⋆⋆ The full list of sources detected in X-rays is given in Table 6 that is only available in electronic form at the CDS via anonymous ftp to cdsarc.u-strasbg.fr (130.79.128.5) or via http://cdsweb.u-strasbg.fr/cgi-bin/qcat?J/A+A/454/595

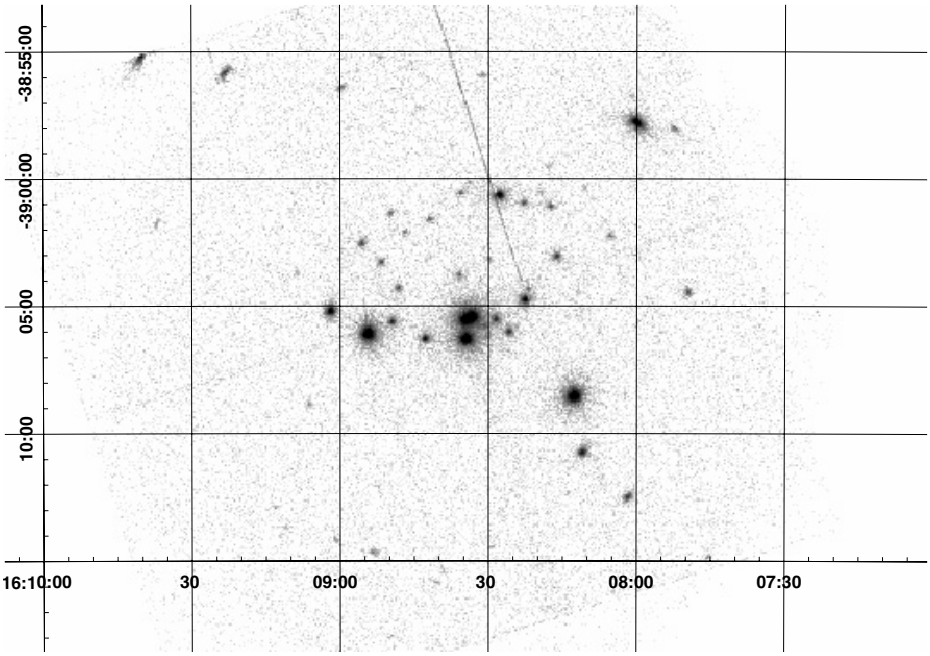

Fig. 1. Combined MOS1, MOS2, and PN image of the Lupus 3 region in the 0.5 to 4.5 keV band. The bright sources in the center of the field of view are HR 6000 (A1.5 III) and the δ Scuti type star HR 5999 (A7IVe).

low mass stars than that found in other star-forming regions (Hughes et al. 1994). I report on the analysis results of an *XMM − Newton* observation of the Lupus 3 region performed in 2003. Section 2 describes the X-ray observations and the data reduction procedure, while Sect. 3 presents the analysis results. Section 4 describes correlations that were found between the X-ray emission of the stars and their main physical parameters. The study results are summarized in Sect. 5.

2. Observation of the Lupus 3 region and source identification

The Lupus 3 region (see Fig. 1) was observed by the *XMM − Newton* space observatory (Jansen et al. 2001) in revolution 685, on 6 September 2003 (see Table 1). The satellite observatory uses three grazing incidence telescopes that provide an effective area higher than 4000 cm^2 at 2 keV and 1600 cm^2 at 8 keV (Gondoin et al. 2000). One CCD EPIC pn camera (Strüder et al. 2001) and two EPIC MOS cameras (Turner et al. 2001) at the prime focus of the telescopes provide imaging in a 30 arcmin field of view and broadband spectroscopy with a resolving power of between 10 and 60 in the energy band 0.3 to 10 keV. Two identical RGS reflection grating spectrometers behind two of the three X-ray telescopes in front of the MOS cameras allow higher resolution ($E/\Delta E$ = 100 to 500) measurements of bright sources in the soft X-ray range (den Herder et al. 2001). The observations of the Lupus 3 region were conducted with the EPIC camera operating in full frame mode (Ehle et al. 2001). The EPIC pn and MOS observations were performed with exposure times of 21 ks and 22.6 ks, respectively. A "thick" aluminum filter was used in front of the EPIC cameras to reject visible light from the stars.

Individual PN, MOS1, and MOS2 images of the Lupus 3 region were built in the 0.5 to 4.5 keV band using all events registered during the observation. The source detection was performed on the individual images, using the standard source detection method of the *XMM − Newton* Science Analysis Software (SAS) that operates in four steps. In a first step, source candidates are identified by a sliding cell method using the SAS package "eboxdetect". A small cell surrounded by a larger cell is moved over the X-ray images. The background counts are estimated from the area surrounding the small cell. If the counts in the small cell are significantly larger than in the background, the cell is considered to have excess counts. The background rate was about 0.015 s^{-1} and 0.05 s^{-1} on average with a maximum value during short time intervals of 0.15 s^{-1} and 0.5 s^{-1} for the MOS and PN, respectively. After sliding the cell over the whole images, these zones of excess counts are considered as source candidates. In a second step, a local background image is created by the SAS package "esplinemap". The source candidates obtained in step 1 are subtracted from the X-ray image, and a spline fit is applied to the resulting image to obtain the background count distribution. In a third step, the sliding cell method is performed again with the SAS package "eboxdetect" to obtain reliable source candidates. This time, only the small size cell is moved over the X-ray images. The local background counts are estimated locally using the background count distribution obtained in the second step. In the last step, a two-dimensional fit is performed on the spatial count distribution of the source candidates by the SAS package "emldetect" using the model of the telescope point spread function and of the background from step 2 and taking into account contamination by nearby sources. The task checks the detection significance of the candidate sources and calculates the count rates and their uncertainties.

As a result of this procedure, 102 X-ray sources were detected with a likely threshold above 12, corresponding to a significance of 4.4σ for a Gaussian statistic, within the 30′ diameter of the EPIC PN, MOS1, and MOS2 fields of view. Hence, the probability is low of a single spurious detection among the 102 sources. The coordinates and count rates corrected for the effective exposure time of the 102 X-ray detected sources are given in Table 6 (in the on-line version only). A significant number of sources are not detected in the MOS1 or MOS2 cameras due to their lower sensitivities and a field

Table 1. Lupus 3 observation log during *XMM − Newton* revolution 685.

Experiment	Filter	Mode	Start Exp.(UT)	Exp. Duration
p−n	Thick	Full Frame	6 September 2003 @ 06:34:02	20 984 s
MOS 1	Thick	Full Frame	6 September 2003 @ 06:11:19	22 617 s
MOS 2	Thick	Full Frame	6 September 2003 @ 06:11:19	22 622 s

Table 2. Counterparts to X-ray sources detected in the EPIC field of view. Column [1] gives the identifying numbers of the sources. Columns [2] and [3] provide the identifiers of IR counterparts from the IRAS and 2MASS catalogues. Columns [4]–[6] provide the identifiers of visible counterparts (with prefix "[KWS97]TTS" or "Lupus 3" from Krautter et al. 1997; with prefix "SZ" from Schwartz 1977; with prefix "[CFB2003]Par-Lup" from Comeron et al. 2003; with prefix [GSC] from the Guide Star Catalogues; with prefix [LEM]Lup from Lopez Marti et al. 2005). The identifiers of previous X-ray detections are indicated under Col. [7]. The *B*, *V* magnitudes (Ochsenbein 1974; Mermilliod 1987) and spectral types (Houk & Cowley 1975; Jaschek 1978) of the counterparts are given in Cols. [8]–[10], respectively.

Id. [1]	IRAS [2]	2MASS [3]	KWS97 [4]	SZ [5]	Other [6]	*ROSAT* Id. [7]	*B* [8]	*V* [9]	Sp. [10]
8			Lupus 3 28	SZ 94			14.6		M4
10				SZ 95			14.2		M1.5
13			TTS 106; Lupus 3 29			RX J1608.0-3857			
22			TTS 107; Lupus 3 30			RX J1608.2-3910	14.10	12.87	K6V
24			Lupus 3 31	SZ 96		1RXS J160814.5-390834	13.2		M1.5
28					[CFB2003] Par-Lup3-1		19.92		M7.5
					[CFB2003] Par-Lup3-1/cc1				M5
36	16050-385			SZ 98			14.4	13.00	K8
37		J16082279-3900591	TTS 111			RX J1608.5-3900B		15.05	M3.5
41				SZ 100			18.09	16.87	M5
44		J16082778-3900406	TTS 110; Lupus 3 35			RX J1608.5-3900A		14.6	M1.5
45				SZ 101			17.03	15.46	M4
50	16051-3855			SZ 102			14.5		K0
59	16052-3858		Lupus 3 41		HR 5999; GSC 07851-01818		7.27	6.98	A7IVe
62					[CFB2003] Par-Lup3-2			16.76	M6
73			Lupus 3 44	SZ 107			15.2		M5.5
74			Lupus 3 45	SZ 108				13.1	M0.5
75					GSC 07851-01158		12.0	11.4	
78				SZ 109			15.6		M5.5
80					[CFB2003] Par-Lup3-3			17.71	M4.5
83				SZ 110			13.6		M2
87			TTS 116; Lupus 3 48		GSC 07851-00426	RX J1608.9-3905	11.9	11.0	K2
88				SZ 112			14.9		M3
92			Lupus 3 50	SZ 114			14.2		M2
94				SZ 115			15.0		M3
95		J16090850-3903430			[LEM2005] Lup 608s		17.8	17.0	M5

dependant vignetting effect of the telescope exit pupils by the Reflection Grating Spectrometers. The source S1 is detected by the MOS cameras, but falls outside of the PN camera field of view. The source HR 6000 (A1.5III) subject of the initial PI observation proposal is not included in Table 6. The detected sources were correlated with the list of Herbig-Haro objects and H_α emission stars from Schwartz (1977) that contains mainly Lupus 3 CTTS, with the catalogue of weak-line TTS in Lupus (Krautter et al. 1997), and with a recent list of new low-mass members of the Lupus 3 dark cloud found in a visible-light spectroscopic survey at the center of the Lupus 3 star-forming core (Comeron et al. 2003). The correlation radius was 4″ based on the astrometric accuracy of the *XMM − Newton* detections. Twenty-four counterparts were found (see Table 2) including two possible candidates Par-Lup3-1 and its companion Par-Lup3-1/cc1 for one single X-ray detection. IR counterparts were searched for in the IRAS (Kleinmann et al. 1986) and in the Two Micron All-Sky Survey (2MASS) catalogues. Only one new counterpart was found; it is known as Lup 608s, a low-mass member of the Lupus 3 cloud recently detected in a multi-band optical survey for very low-mass stars and brown dwarfs in the Lupus clouds (Lopez Marti et al. 2005). Correlation with visible catalogues including the Guide Star Catalog (Lasker et al. 1990) lead to one last counterpart identification (GSC 07851-01158) not listed as a member of the region, although its magnitude, color index, and proper motion are not inconsistent with Lupus membership. Only 6 sources were detected previously in X-ray, namely TTS 106, TTS 107, Lupus 3 31, TTS 110, TTS 111, and TTS 116 (Krautter et al. 1997). Of special interest are the 14 stars (Sz 94, Sz 95, Sz 96, Sz 98, Sz 100, Sz 101, Sz 102, Sz 107, Sz 108, Sz 109, Sz 110, Sz 112, Sz 114, and Sz 115) studied in detail by Hughes et al. (1994) and the four low-mass members (Par-Lupus3-1, Par-Lupus3-1/cc1, Par-Lupus3-2, and Par-Lupus3-3) recently discovered by Comeron et al. (2003).

3. Analysis

3.1. Spectral fitting of the brightest X-ray sources

The light curves and spectra (see Figs. 2 and 3) of the brightest X-ray sources with known TTS counterparts (see Table 2) were built from photons detected with the PN camera within windows of about 30″ diameter around the targets. The background was estimated on the same CCD chips as the sources, within windows of the same sizes offset from the source positions in empty field regions. The light curves were accumulated

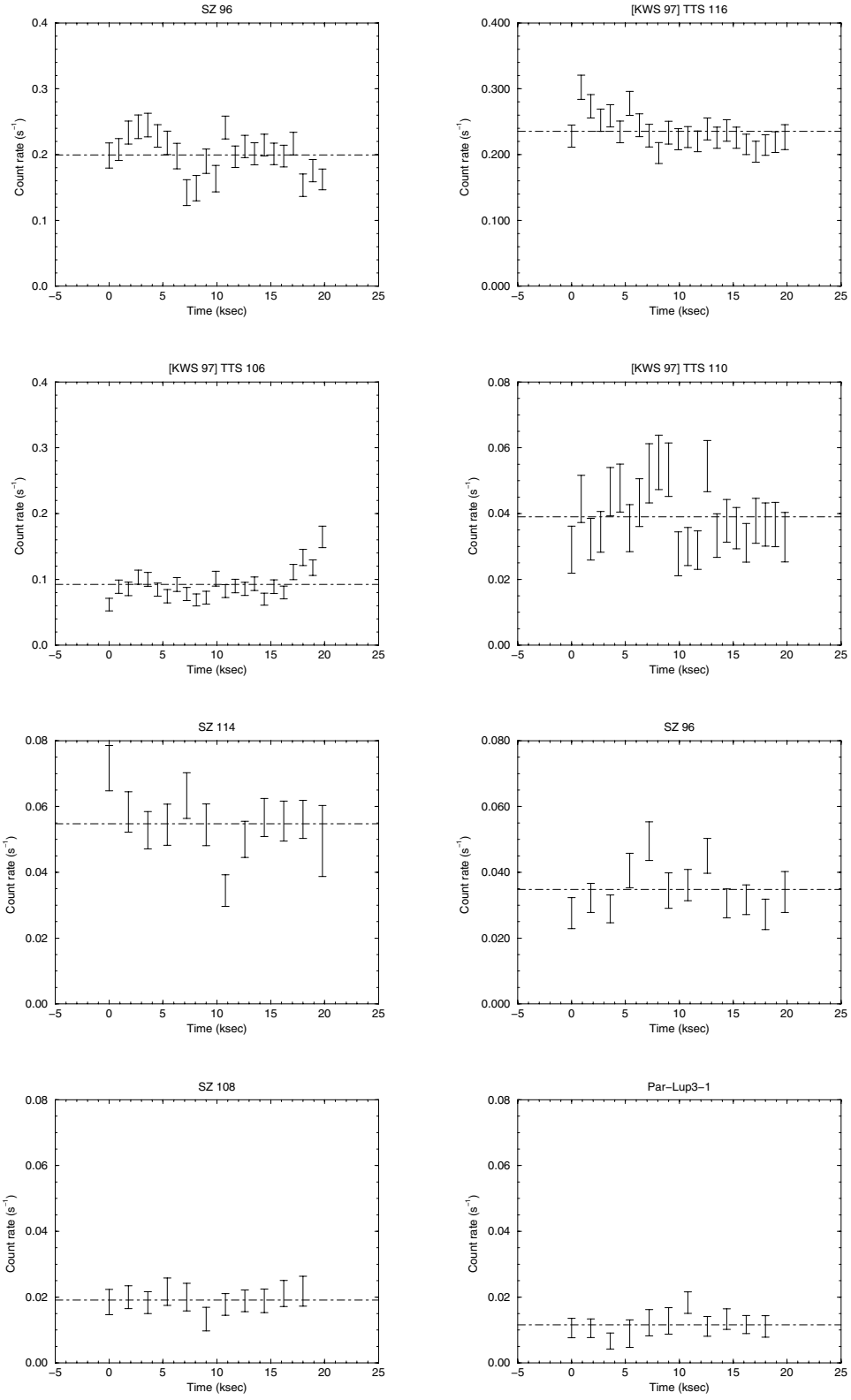

Fig. 2. Light curves of the X-ray brightest TTS detected in the Lupus 3 subgroup. The curves represent the count rates in the 0.5 to 4.5 keV band. The *X*-axis is the time since the beginning of the observation. Events are binned in 900 s time intervals for SZ 96, TTS 106, TTS 110, and TTS 116 and in 1800 s time intervals for the other sources. Bars represent a $\pm 1\sigma$ error on the count rates within a time bin.

in the 0.5 to 4.5 keV band. To remove variable contributions from the background, the background light curves were subtracted from the light curves of the sources using the "lcmath" program of the XRONOS general purpose timing analysis package (Johnson 2004). The calibrated light curves were then tested for variability using the XRONOS task "lcstats" that performs

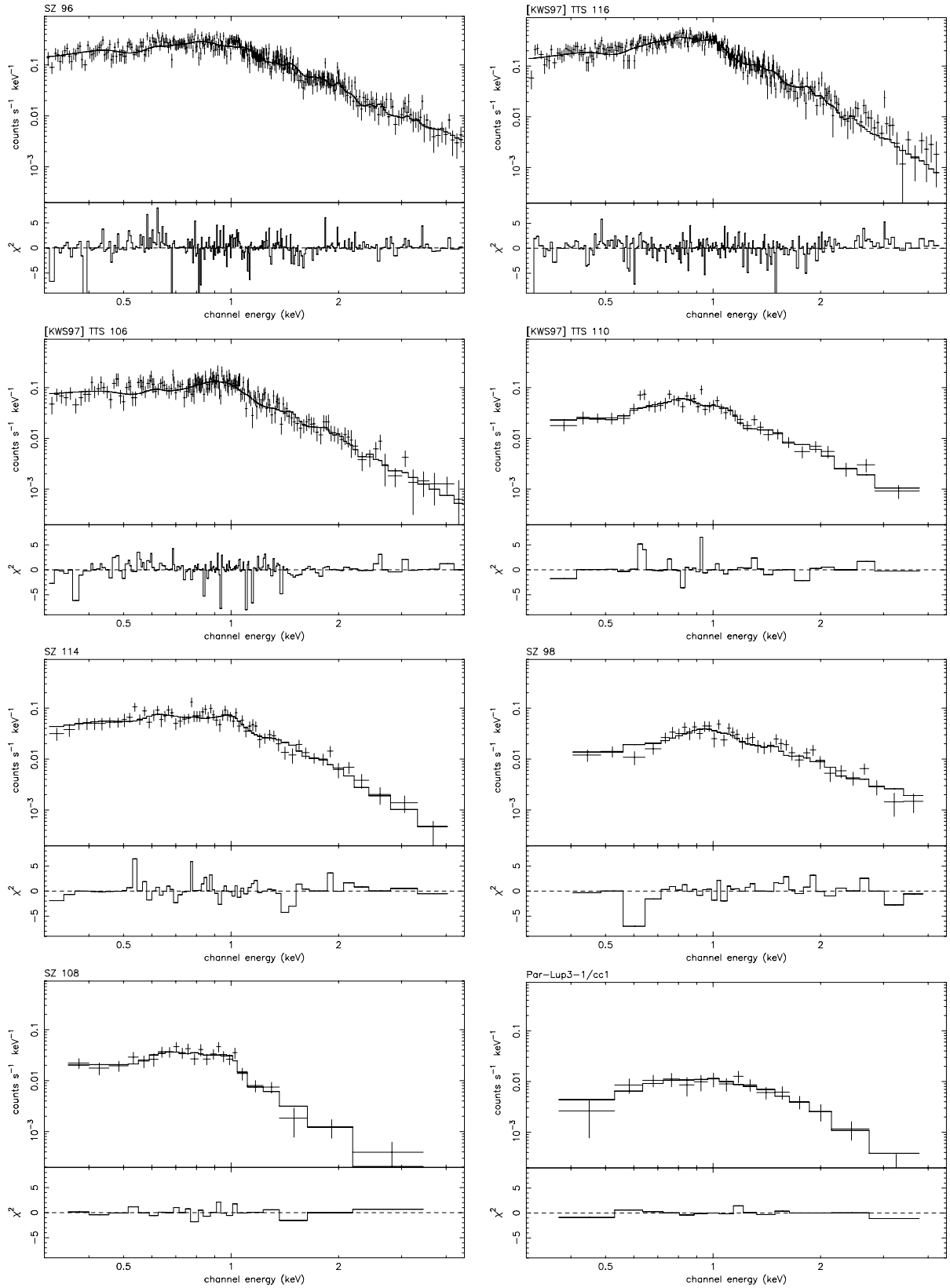

Fig. 3. Best-fit models to the EPIC PN spectra of the X-ray brightest sources in the Lupus 3 subgroup. The names of the stars are indicated on the top of each graph. The EPIC data (crosses) and spectral fit (solid line) are shown in the upper panel of each graph and the χ^2 contributions in their lower panel.

a Kolmogorov-Smirnov test on binned light curves. None of the X-ray bright sources displayed a light curve compatible with that of a constant source.

The Pulse-Invariant (PI) spectra of the brightest X-ray sources were rebinned such that each resulting channel had at least 10 to 20 counts per bin depending on source counts.

Table 3. Best-fit parameters to the EPIC spectra using a two components MEKAL model (Mewe et al. 1985) with variable abundance and with a hydrogen column density derived from the visual extinction.

Source	Id	$N_{\rm H}$ (10^{20} cm^2)	Z	$kT_{\rm cool}$ (keV)	$EM_{\rm cool}$ (10^{52}cm^{-3})	$kT_{\rm hot}$ (keV)	$EM_{\rm hot}$ (10^{52}cm^{-3})	χ^2
13	TTS 106	1.8	0.25 ± 0.05	0.79 ± 0.04	7.2 ± 3.2	1.6 ± 0.2	11.5 ± 2.5	1.00
24	SZ 96	8.9	0.06 ± 0.01	0.67 ± 0.02	37.8 ± 5.0	3.0 ± 0.2	14.1 ± 1.5	1.12
28	ParLup3-1/cc1	0.0	1.0	0.25 ± 0.05	2.4 ± 2.1	1.8 ± 0.4	2.2 ± 0.5	0.76
36	SZ 98	14.6	1.0	0.86 ± 0.09	0.4 ± 0.2	4.25 ± 0.92	3.8 ± 0.5	1.16
44	TTS 110	5.5	0.8 ± 0.4	0.64 ± 0.03	0.9 ± 0.7	2.3 ± 0.3	3.1 ± 1.0	1.02
74	SZ 108	0.0	0.4 ± 0.2	0.37 ± 0.06	0.9 ± 0.7	0.99 ± 0.09	1.0 ± 0.7	0.75
87	TTS 116	9.2	0.16 ± 0.02	0.59 ± 0.03	21.4 ± 4.4	1.17 ± 0.06	2.5 ± 0.4	1.15
92	SZ 114	9.2	0.12 ± 0.04	0.29 ± 0.03	7.8 ± 3.0	1.14 ± 0.08	10.3 ± 2.7	1.07

An EPIC response matrix and an ancillary response file that includes an aperture correction were generated by the SAS task "rmfgen" and "arfgen" for each individual source. All fits were performed using the XSPEC package (Arnaud & Dorman 2001), and χ^2 minimization was used for spectral fitting. The spectral fitting was performed in the 0.3–4.5 keV spectral band with a MEKAL optically thin plasma emission model (Mewe et al. 1985). The WABS model for photoelectric absorption was used to take extinction by the interstellar medium into account. The neutral hydrogen column density $N_{\rm H}$ was estimated from the visual extinction $A_{\rm V}$ using the relation $N_{\rm H}$ (cm^{-2})/$A_{\rm V}$ = 1.774 × 10^{21} following the detailed investigation of absorption in the local environment of T Tauri stars by Paresce (1984) and Vrba & Rydgren (1985). The visual extinctions were obtained from Hughes et al. (1994) for Sz 96, Sz 98, Sz 108, and Sz 114, from Krautter et al. (1997) for TTS 106, TTS 110, and TTS 116 and from Comeron et al. (2003) for Par-Lup3-1/cc1. No single temperature plasma model that assumes either solar photospheric (Anders & Grevesse 1989) or non-solar abundances can fit the spectra of Sz 96, Sz 98, Sz 108, Sz 114, TTS 106, TTS 110, and TTS 116, as unacceptably large values of χ^2 are obtained. A MEKAL plasma model with two components at different temperatures, but having the same metallicity, proves acceptable for all data. The best-fit parameters of the two temperature components plasma model are given in Table 3. The emission measures of the different plasma components in the X-ray brightest sources of the Lupus 3 region are of the order of 10^{52} cm^{-3}, in agreement with the emission measure values of coronal plasma observed in some T Tauri stars stars (Argiroffi et al. 2005; Stelzer & Schmitt 2004) for which high resolution X-ray spectra could be obtained because they are bright and close enough. A comparison with the much larger sample of PMS stars detected in the Orion Nebula Cluster by the COUP project (Getman et al. 2005; Feigelson et al. 2005) suggests that these objects are not representative of the general PMS population. The emission measure of the X-ray bright Lupus 3 stars is intermediate between that of the bulk of the COUP sources and the brightest in the COUP sample, likely because this latter is much larger than that of the Lupus 3 region. Emission measure values similar to those measured on the X-ray brightest Lupus 3 TTS are found in post-T Tauri stars (Argiroffi et al. 2004) and in late-type dwarfs that are members of close binary systems (e.g., Gondoin 2004a,b).

Spectral fitting of EPIC data yields flux measurements in the 0.3−2 keV and 2−4.5 keV bands. These measurements were converted into X-ray luminosities $L_{0.3-2\ \rm keV}$ and $L_{>2\ \rm keV}$ using a distance d = 140 pc (Hughes et al. 1993). Table 4 gives the X-ray luminosities of the stars and the hardness ratios hr of their X-ray emission defined as $hr = (L_{>2\ \rm keV} - L_{0.3-2\ \rm keV})/(L_{>2\ \rm keV} + L_{0.3-2\ \rm keV})$. The X-ray luminosities, plasma temperatures, and emission measures in Lupus 3 X-ray brightest TTS are comparable to those of rapidly rotating main-sequence stars in close binary systems. Isolated main-sequence stars generally have lower activity levels.

Table 4. X-ray luminosities of the X-ray brightest T Tauri stars detected in the Lupus 3 "star-forming" region in the 0.3−2.0 keV and 2−4.5 keV energy bands corrected for interstellar absorption.

Source	Id.	$L_{0.3-2\ \rm keV}$	$L_{2-4.5\ \rm keV}$	hr
	(10^{29} erg s^{-1})	(10^{29} erg s^{-1})		
13	TTS 106	14.8	2.7	–0.69
24	SZ 96	31.0	7.3	–0.62
28	ParLup3-1/cc-1	3.9	0.56	–0.75
36	SZ 98	4.0	2.0	–0.34
44	TTS 110	4.8	1.2	–0.60
74	SZ 108	2.0	0.11	–0.90
87	TTS 116	32.2	3.2	–0.82
92	SZ 114	9.6	1.0	–0.81

One property of the X-ray brightest stars in Lupus 3 that distinguish them from normal late-type stars is the low abundance of Fe obtained where abundance is left as a free parameter in the spectral fitting. The peculiar chemical compositions and in particular low Fe abundance noticed in some T Tauri stars may be due to the composition of the original molecular cloud that formed the stars or to a settling of dust in a circumstellar disk (Argiroffi et al. 2005; Stelzer & Schmitt 2004). Dust continuum emission at mm wavelength from Lupus 3 TTS has been reported (Nürnberger et al. 1997) and strong H_α and CaII infrared triplet emission in the spectra of many Lupus 3 stars is interpreted as a tracer of accretion processes (Comeron et al. 2003). Low coronal abundances seems to be the norm rather than the exception for PMS stars (e.g., Imanishi et al. 2001a; Getman et al. 2005) and, in general, little relation has been found between abundances and accretion. The spectral fits of the X-ray brightest TTS in Lupus 3 do not support such a relation, given that the star with the lowest abundances is a WTTS (SZ 96; see Table 4). Moreover, low abundances are also found in more evolved, but still very active 40–100 Myr old stars that do not accrete any longer, e.g., in the Pleiades (Briggs et al. 2003), in Bianco 1 (Pillitteri et al. 2004), and in IC 2391 (Marino et al. 2005).

Most X-ray bright sources in Lupus 3 exhibit a hard X-ray spectrum with a flux above 2.0 keV that sometimes exceeds 20% of the flux in the 0.3–2.0 keV band. Hot plasmas at temperatures in the range (1–50) × 10^7 K contribute to most of the luminosity above 2 keV. Their emission measure is comparable and sometimes larger that those of the cool plasma components at (3–10) × 10^6 K. Although accreting material may provide a heating mechanism for the emitting plasma, shock-heated

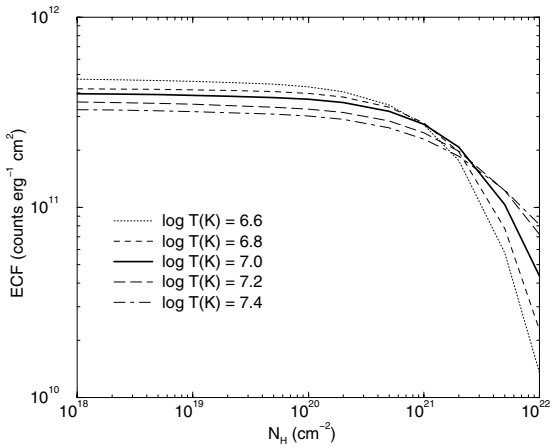

Fig. 4. Energy conversion factor in the 0.5–4.5 keV energy range for the EPIC pn camera equipped with a thick filter versus the hydrogen column density. The energy conversion factor was calculated using an emission model of optically thin plasmas with temperatures ranging from $10^{6.6}$ to $10^{7.4}$ K.

plasma cannot attain temperatures higher than a few MK. The evidence for hot plasma components with large emission measures indicates that accretion shocks provide at most a moderate contribution to the X-ray emission of the brightest Lupus 3 stars. In active stellar coronae, it has been proposed that the peak in emission measure around 10^7 K is due to flaring activity (Drake et al. 2000; Sanz-Forcada et al. 2002). The large emission measure of hot ($T > 10^7$ K) plasma in Lupus 3 TTS may thus be caused by disruptions of magnetic fields associated with an intense flaring activity, while the X-ray emission from the "cool" $T \approx 3$–9×10^6 K plasma components may result from solar-type active regions. As commonly interpreted for WTTS, the origin of the X-ray emission in the X-ray brightest Lupus 3 TTS could be a scaled-up solar-type magnetic activity.

3.2. Estimates of X-ray luminosities

To estimate the X-ray luminosities of the faintest sources from their count rates, I calculated energy conversion factors for the EPIC pn camera (see Fig. 4) using the Portable, Interactive, Multi-Mission Simulator (PIMMS; Mukai 1993) in the 0.5–4.5 keV range for optically thin plasmas with temperatures comparable to those found in the spectral fitting of the brightest sources (see Table 3). For absorbing hydrogen column densities lower than 10^{21} cm^{-2}, the energy conversion factor in the 0.5–4.5 keV band is flat and well-approximated by ECF = 3.7×10^{11} counts erg^{-1} cm^2 for plasma temperatures in the range (4–25) $\times 10^6$ K. For converting the count rates of faint sources that could not be studied spectroscopically into X-ray luminosities, a 10^7 K optically thin plasma was assumed that is absorbed by an hydrogen column density derived from the visual extinction A_V (Hughes et al. 1994; Krautter et al. 1997; Comeron et al. 2003; see Sect. 3.1). This procedure was also used to estimate the upper limits of the X-ray luminosities of known low-mass stars in the EPIC field of view that were not detected in X-rays. The count rate upper limits of these sources were derived as follows. First, event numbers $N_{\rm src+bgd}(r)$ were estimated within extraction windows of radius r centered on the x, y detector position of each undetected source. For each value $N_{\rm src+bgd}(r)$, the approximate formula $N^{\rm ul}_{\rm src+bgd}(r) = N_{\rm src+bgd}(r) + S \times \sqrt{N_{\rm src+bgd}(r)1 + (S^2+2)/3}$ (Gehrels 1986) was used to calculate the 99.9989% confidence level upper limit $N^{\rm ul}_{\rm src+bgd}(r)$ that corresponds to the $S = 4.4\sigma$ in Gaussian statistics selected for the source detection algorithm. For each position of undetected source, the local average background $\langle B \rangle$ per window of radius r was then estimated, assuming a uniform background. Finally, the upper limit of the source count rate was calculated as follows:

$$CR^{\rm ul}_{\rm src} = \frac{N^{\rm ul}_{\rm src+bgd}(r) - \langle B \rangle}{EE(r) \times V(x,y) \times t_{\rm exp}} \quad (1)$$

where $EE(r)$ is the encircled energy fraction within a radius r of the telescope point spread function at the (x, y) source location within the telescope's field of view. $V(x, y)$ is a vignetting function that was calculated with the SAS command "eexpmap" and normalized to its on-axis value. $t_{\rm exp}$ is the exposure time (see Table 1). Table 5 gives the X-ray luminosities and upper limits of all stars in EPIC's field of view that are known from the catalogues of Schwartz (1977), Krautter et al. (1997), and Comeron et al. (2003). Table 5 also provides their bolometric luminosities, effective temperatures, masses, ages, H_α equivalent widths, and $\Delta(H - K)$ color excesses.

The effective temperatures and bolometric luminosities derived from the catalogues of Hughes et al. (1994), Krautter et al. (1997), and Comeron et al. (2003), were used to place the stars in an HR diagram (see Fig. 5) and to compare their positions with evolutionary models of solar metallicity low-mass stars computed by Baraffe et al. (1998; hereafter B98). The comparison yields estimates of masses and ages. The median mass is about 0.2 $M_\odot$ and the mass vs. age diagram (see Fig. 6) shows that all stars more massive than 0.5 $M_\odot$ were detected in X-rays. X-ray emission was detected from stars with high bolometric luminosities, i.e., preferably from the more massive or from the youngest stars. Three objects in the observed Lupus 3 region (SZ 107, SZ 109, and Par-Lup3-1) have mass estimates lower than the brown dwarf limit of about 0.075 $M_\odot$ for solar metallicity. These mass estimates are, however, uncertain since the HR diagram positions of these candidate brown dwarfs fall outside the B98 evolutionary tracks. Remarkably, two of these young (age < 1 Myr) and low-mass objects, namely SZ 107 and SZ 109, are emitting X-rays with a luminosity of about 4–7 $\times$ 10^{28} erg s^{-1}. Young brown dwarfs are known to emit in X-rays (Neuhäuser & Comeron 1998; Neuhäuser et al. 1999; Imanishi et al. 2001a,b; Preibisch & Zinnecker 2001; Mokler & Stelzer 2002; Feigelson et al. 2002; Tsuboi et al. 2003). From the first spectral analysis of a flaring brown dwarf, Ozawa et al. (2005) derived an X-ray luminosity of $L_{\rm X} = 19 \times 10^{28}$ erg s^{-1}, comparable with the X-ray luminosity estimates of SZ 107 and SZ 109.

4. Discussion

This section describes the X-ray properties as a function of stellar parameters of a sample of stars within the EPIC field of view that were known prior the *XMM − Newton* observation. The sample (see Table 5) consists of all stars in the EPIC field of view known from the catalogues of Schwartz (1977), Krautter et al. (1997), and Comeron et al. (2003). It is biased towards CTTS since 66% of the stars were identified in the H_α survey performed by Schwartz (1977). Some of the H_α survey sources identified by this author reach a V magnitude $m_V \approx 17.5$ (Hughes et al. 1994). The X-ray survey of Krautter et al. (1997) excludes all X-ray sources without a stellar counterpart of R magnitude $m_R \leq 15$, which converts to $m_V \leq 16$ for an M2V star.

Table 5. Properties of known low-mass TTS in the EPIC field of view. Column [2] is the source name (with prefix "SZ" from Schwartz 1977, "TTS" from Krautter et al. 1997, and "Par-Lup" from Comeron et al. 2003). Column [3] gives the spectral type. Columns [10] and [11] provide the the H_α equivalent width and the $\Delta(H-K)$ color excess from Hughes et al. (1994), Wichmann et al. (1997b), and Comeron et al. (2003).

S	Id	Sp.	L_X (10^{28} erg s^{-1})	L_{bol} ($L_\odot$)	L_X/L_{bol} (10^{-3})	T_{eff} (K)	M ($M_\odot$)	Age (10^6 yr)	W_{H_α} (Å)	$\Delta(H-K)$
[1]	[2]	[3]	[4]	[5]	[6]	[7]	[8]	[9]	[10]	[11]
8	SZ 94	M4	8.3 ± 0.7	0.07	0.31	3150	0.18	2.6	7.3	–0.01
10	SZ 95	M1.5	13.0 ± 1.6	0.18	0.19	3570	0.53	5.7	10.2	0.03
13	TTS 106	M0	128.5 ± 3.2	0.38	0.88	3800	0.86	6.4		0.02
22	TTS 107	K6	26.6 ± 1.3	0.28	0.25	4260	0.88	28		0.03
24	SZ 96	M1.5	278.0 ± 4.0	0.29	2.51	3570	0.55	3.6	1.0	0.20
28	Par-Lup3-1	M7.5	7.9 ± 0.6	0.05	0.41	2760	0.04*	<1**	12	
	Par-Lup3-1/cc1									
36	SZ 98	K8	43.5 ± 1.8	0.62	0.18	3800	0.90	2.9	29.1	0.55
37	TTS 111	M3.5	6.6 ± 1.1	0.06	0.29	3950	0.60	147		0.03
41	SZ 100	M5	18.5 ± 1.2	0.12	0.40	3000	0.10*	<1**	21.4	0.14
44	TTS 110	M1.5	51.9 ± 1.7	0.14	0.97	3570	0.52	8.5		0.03
45	SZ 101	M4	20.9 ± 1.3	0.19	0.29	3150	0.17	1.0	26.0	–0.08
50	SZ 102	K0	3.8 ± 0.7	0.01	0.86				377.4	1.01
62	Par-Lup3-2	M6	4.3 ± 0.5	0.20	0.06	2970	0.09*	<1**	6.5	
73	SZ 107	M5.5	4.0 ± 0.5	0.07	0.15	2900	0.07*	<1**	16.1	–0.02
74	SZ 108	M0.5	17.8 ± 0.9	0.44	0.11	3650	0.69	3.1	0.5	0.11
78	SZ 109	M5.5	7.0 ± 0.7	0.07	0.26	2900	0.06*	<1**	21.7	0.06
80	Par-Lup3-3	M4.5	27.7 ± 2.2	0.63	0.11	3420	0.53	1.0	19	
83	SZ 110	M2	14.6 ± 1.4	0.17	0.22	3500	0.45	5.1	60.1	0.13
87	TTS 116	K2	318.2 ± 5.7	0.76	1.09	4900	1.04	26		0.06
88	SZ 112	M3	18.3 ± 1.4	0.14	0.34	3150	0.19	1.4	46.7	0.16
92	SZ 114	M2	90.4 ± 2.9	0.22	1.07	3150	0.17	1.0	33.0	0.13
94	SZ 115	M3	3.1 ± 0.5	0.08	0.10	3150	0.19	2.9	7.1	0.05
	SZ 97	M3	<3.8	0.13	<0.08	3350	0.31	3.2	58.2	0.00
	SZ 99	M3.5	<4.7	0.08	<0.15	3250	0.23	4.5	49.8	0.02
	SZ 103	M4	<2.7	0.06	<0.12	3150	0.18	3.4	33.1	0.21
	SZ 104	M5.5	<2.7	0.05	<0.14	3000	0.10	2.1	13.3	0.12
	SZ 106	K8	<3.5	0.03	<0.30	3800	0.50	>250	81.7	0.72
	SZ 113	M1.5	<4.7	0.03	<0.41	3150	0.14	5.7	160.1	0.12
	Par-Lup3-4	M5e	<13.8	0.006	<6.0	3125	0.11	35	410	

* Uncertain mass estimate; ** uncertain age estimate.

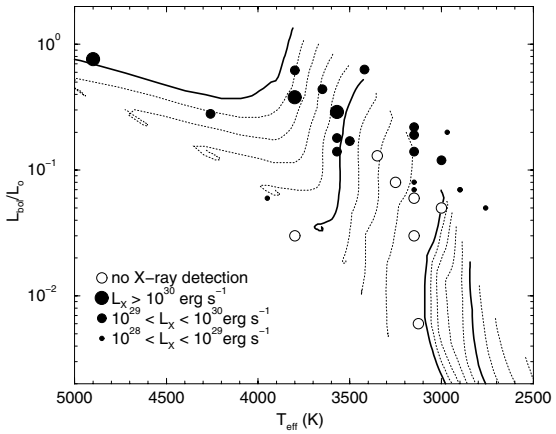

Fig. 5. H-R diagram of low mass stars in the EPIC field of view compared to evolutionary tracks (Baraffe et al. 1998). The solid lines from right to left describe the evolutionary tracks of 0.05 $M_\odot$, 0.1 $M_\odot$, 0.5 $M_\odot$, and 1.0 $M_\odot$, respectively. Black circles mark the position of stars detected with *XMM − Newton*. Their size is indicative of the X-ray luminosity as described in the legend. Open circles mark stars that have not been detected in X-rays.

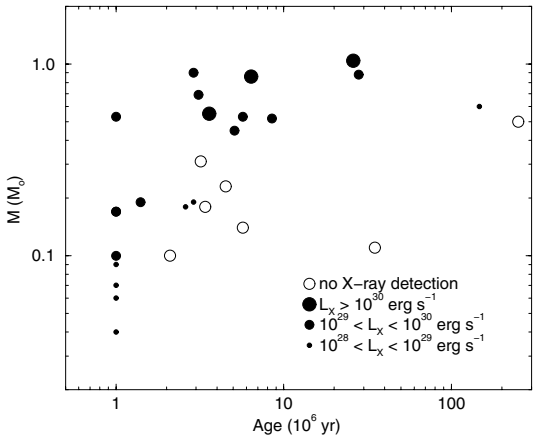

Fig. 6. Mass vs. age diagram of known low mass stars in the EPIC field of view. Black circles mark stars that have been detected in X-rays. Ages marked as 1 Myr are actually upper limits.

4.1. X-ray emission vs. bolometric luminosity and effective temperature

Figure 7 shows a plot of the X-ray luminosities including upper limits versus the bolometric luminosities of the Lupus 3 stars. All stars with bolometric luminosities greater than 0.13 $L_\odot$ were detected in X-rays. The X-ray detected stars have $\log(L_X/L_{bol}) > -4.2$ and are therefore more X-ray active than the Sun for which $\log(L_X/L_{bol}) \approx -6.5$ is an average during the course of the solar cycle. For the most active stars (e.g., TTS 106, TTS 110, and TTS 116), $\log(L_X/L_{bol}) \approx -3$, which is known as the "saturation limit" for coronally active stars (Fleming et al. 1989;

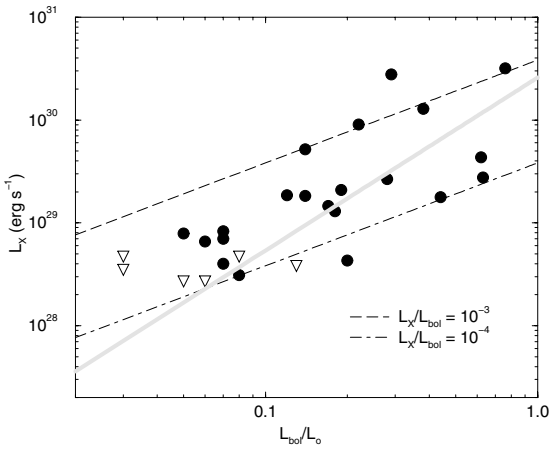

Fig. 7. X-ray luminosities vs. bolometric luminosities of known low mass stars in the EPIC field of view. Black circles mark X-ray detections and triangles mark upper limits. The thick gray line shows the EM algorithm regression fit computed with ASURV (see text).

Patten & Simon 1996; Randich et al. 2000; Pizzolato et al. 2003). Only one star (SZ 96; M1.5) exceeds this saturation limit, possibly because it was flaring during the observation, as suggested by its light-curve variability. A correlation between L_X and L_{bol} is noticeable in Fig. 7 with, however, a large scatter. A linear regression to the L_X vs. L_{bol} plot for X-ray detected sources (i.e., excluding upper limits) yields $\log(L_X[\mathrm{erg\ s^{-1}}]) = 30.0(\pm0.2) + 0.9(\pm0.2) \times \log(L_{bol}/L_\odot)$ with a standard deviation of 0.58 in $\log(L_X)$. This relation is similar to the relation found for other young clusters (see Feigelson & Montmerle 1999) and is consistent with a linear relation between X-ray and bolometric luminosity characterized by $\langle\log(L_X/L_{bol})\rangle = -3.5 \pm 0.4$. However, the L_X/L_{bol} upper limits for the Lupus stars that were not detected in X-rays are most often lower than this value. Hence, I used the ASURV analysis package (Feigelson & Nelson 1985; Isobe et al. 1986; LaValley et al. 1990) for a statistical investigation of the relation between L_X and L_{bol}, taking into account not only X-ray detections, but also upper limits of the X-ray luminosity. The ASURV software provides the maximum-likehood estimator of the censored distribution, several two-sample tests, correlation tests, and linear regressions. The linear regression fit with the parametric estimation maximization (EM) algorithm in ASURV yields $\log(L_X[\mathrm{erg\ s^{-1}}]) = 30.4(\pm0.2) + 1.7(\pm0.3) \times \log(L_{bol}/L_\odot)$, suggesting that the relation between L_X and L_{bol} is no longer linear when X-ray faint objects are taken into account. It is worth noting that this relation is much steeper than the linear regression fit to $\log(L_X)$ vs. $\log(L_{bol})$ (slope = 0.42 ± 0.05) found by Preibisch et al. (2005) for a sample of nearby G-, K-, and M-type field stars. The relation is also steeper than the linear regression fit to $\log(L_X)$ vs. $\log(L_{bol})$ (slope = 1.04 ± 0.06) found by the same authors for the Orion Nebula Cluster stars that are similar in age to Lupus 3 members. The difference could result from the bias in the selection of the Lupus sample that is based for the most part on an H_α survey. This bias is especially important among stars with X-ray upper limits (see Table 5) that are responsible for increasing the slope from 0.9 to 1.7 (see Fig. 7). This also suggests a difference between accreting and non-accreting stars with a steeper slope for the accreting stars that dominate the Lupus 3 sample. Preibisch et al. (2005) find two different relations for accretors and non-accretors, but with an opposite effect on the $\log(L_X)$ vs. $\log(L_{bol})$ relation since the non-accretors in the ONC show a steeper power-law slope. However, these authors noted that the accreting stars show a scatter in $\log(L_X)$ vs. $\log(L_{bol})$ correlation considerably larger than expected from X-ray variability. They argue that some fraction of this scatter may be due to the fact that the more rapidly accreting stars may have large errors in stellar luminosity and effective temperature values due to the effect of accretion on the observables that lead to these quantities.

The X-ray surface fluxes (i.e., X-ray luminosities divided by the stellar surface area) of the Lupus 3 stars are included between 10^5 and 10^8 erg s^{-1} cm^{-2}. These values are comparable with the range of X-ray fluxes found for different structures in the solar corona. Coronal holes show X-ray fluxes around 10^4 erg s^{-1} cm^{-2}, while active regions show fluxes of up to 10^8 erg s^{-1} cm^{-2}. The similarity of the X-ray surface flux range for late-type stars and for different constituents of the solar corona have already been noted, e.g., in Schmitt (1997) and in Peres et al. (2004). The X-ray surface fluxes strongly decrease at effective temperatures below 3500 K, corresponding to M-type stars. This effect results from the dependence $F_X = \sigma T_{eff}^4 \times L_X/L_{bol}$, in which σ is the Stefan-Boltzmann constant and L_X/L_{bol} does not vary much with T_{eff}.

4.2. X-ray luminosity vs. mass and volume

Mass estimates from PMS evolutionary models are subject to significant uncertainties (Baraffe et al. 2002). Different models or temperature scales can lead to differences of as much as a factor of 2 in the mass estimates (e.g., Luhman 1999; Hillenbrand & White 2004). As a test to what extent the L_X vs. mass relation is dependant on the choice of the model, I compared the relation found for the masses derived from the B98 models to those based on stellar masses estimated by Hughes et al. (1994) from D'Antona & Mazzitelli (1994; DM94 hereafter) evolutionary tracks that used the Canuto & Mazzitelli (1992) convection model and opacities from Alexander et al. (1991). Mass estimates from DM94 tracks (Hughes et al. 1994) are only available for the Schwartz (1977) sample stars. A clear correlation is found between X-ray luminosities and masses (see Fig. 8, left) estimated from either the DM94 or B98 evolutionary tracks. The B98 model leads to an EM linear regression fit of $\log(L_X[\mathrm{erg\ s^{-1}}]) = 29.6(\pm0.2) + 0.9(\pm0.3) \times \log(M/M_\odot)$ with a standard deviation of 0.60, while the DM94 yields a relation $\log(L_X[\mathrm{erg\ s^{-1}}]) = 29.7(\pm0.6) + 1.3(\pm0.8) \times \log(M/M_\odot)$ with a standard deviation of 0.67. The B98 and DM94 models thus give consistent L_X vs. mass dependences with power-law slopes similar to those found for TTS in the Orion Nebula Cluster and for nearby G-, K-, and M-type field stars (Preibisch et al. 2005). These slopes of 0.9 and 1.3 are lower than those found for the Chameleon star-forming region (slope = 3.6 ± 0.6 in the mass range 0.6–2 $M_\odot$; Feigelson et al. 1993), for the very young stellar cluster IC 348 (slope = 2.0 ± 0.2 in the mass range 0.1–2 $M_\odot$; Preibisch & Zinneker 2002), or for that derived for M-type field stars (slope = 2.5 ± 0.5 in the mass range 0.15–0.6 $M_\odot$; Fleming et al. 1988). The differences in slopes are in part due to differences in the considered mass ranges and in the methods used to estimate stellar masses. Also, studies prior to *XMM − Newton* and *Chandra* had to deal with large numbers of X-ray upper limits, which perhaps caused the typical X-ray luminosities of very low-mass stars to be underestimated (Preibisch et al. 2005).

The X-ray luminosities of the Lupus TTS also show a correlation with the stars' internal volumes (see Fig. 8, right). The EM linear regression fit gives $\log(L_X[\mathrm{erg\ s^{-1}}]) = 28.9(\pm0.1) + 0.9(\pm0.3) \times \log(V/V_\odot)$ with a standard deviation of 0.59. This suggests a magnetic flux dependence on mass and volume. Although the dependence on mass may be unexplained, the

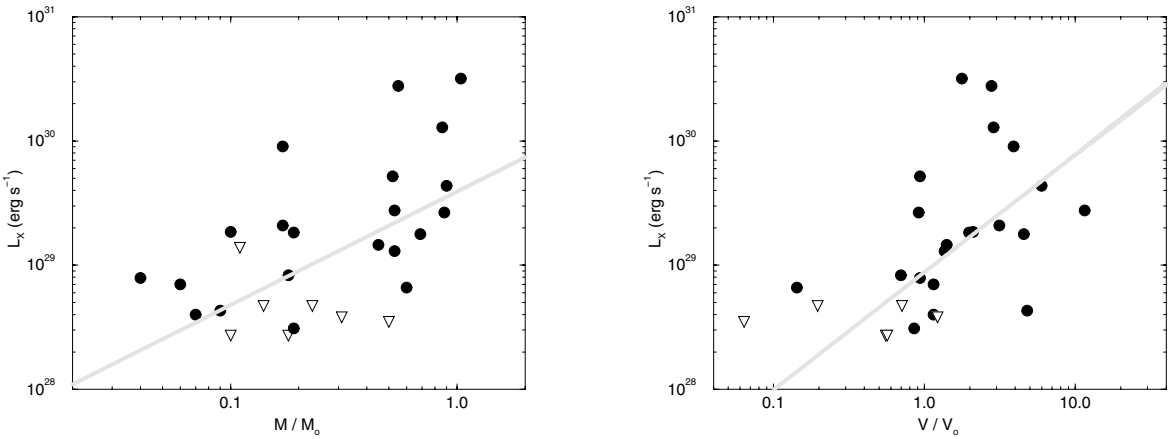

Fig. 8. X-ray luminosities vs. masses (*left*) estimated from B98 evolutionary models and versus volumes (*right*) for known low-mass stars in the EPIC field of view. Black circles represent X-ray detection and triangles indicate upper limits. The thick gray lines show the EM algorithm regression fit computed with ASURV (see text).

importance of volume is qualitatively expected from some models of distributed turbulent dynamos, where the magnetic field is both generated and transported in the convection zone. Such a dynamo could be an important source of magnetic activity in Lupus 3 TTS that are most likely fully convective, and for which the standard solar-like $\alpha - \Omega$ dynamo, which is anchored at the boundary between the convective envelope and the inner radiative core, should not work. Several studies, however, indicate that accretion could change the stellar structure (Prialnik & Livio 1985; Wuchterl & Tscharnuter 2003) so that even for moderate accretion rates, the stars are no longer fully convective. Quantitative relationships between magnetic field generation and stellar parameters for the candidate dynamo mechanisms would be needed to understand the meaning of L_X vs. mass or volume correlation in Lupus 3 TTS.

4.3. X-ray luminosity vs. H_α emission and IR excess

X-ray activity is known to be present during the evolution of pre-main sequence stars both in the initial evolutionary stage of a "classical T Tauri Star" (CTTS), during which the star has an accretion disk that surrounds it, and in the subsequent "weak line T Tauri Star" (WTTS) phase in which the star has no accreting material and is approaching the zero-age main sequence (Feigelson & Montmerle 1999). The origin of the X-ray emission from WTTS is commonly interpreted in terms of scaled-up solar-type magnetic activity, but the situation is less clear for the accreting CTTS. While nothing should prevent the formation of magnetic fields and ensuing coronae in CTTS, X-rays could also be produced above the circumstellar disk or at the star-disk interface, e.g., above the hot spot where a magnetically funneled accretion flow impacts on the stellar surface (Lamzin et al. 1996). One way to separate CTTS from WTTS consists of using the H_α emission and the IR excess emission $\Delta(H-K)$ calculated by de-reddening the observed colors and subtracting the color of the photosphere of the correct spectral type (Hughes et al. 1994). The infrared excess emission is a tracer of circumstellar material, while H_α line emission is thought to be a tracer of accretion. CTTS are often defined as having an H_α equivalent width greater than 10 Å. Among the 18 known CTTS in the EPIC field of view, 12 were detected in X-rays. Figure 9 plots the logarithm of the H_α equivalent width against the IR excess emission $\Delta(H-K)$ of known low-mass stars in the EPIC field of view. Figure 9 shows that most of the known TTS in the EPIC field of

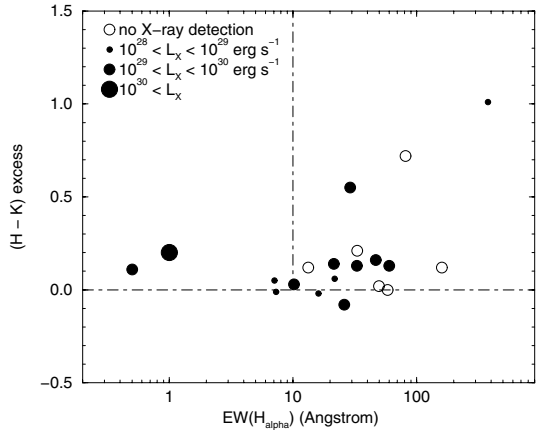

Fig. 9. Logarithm of the H_α equivalent width against the IR excess emission $\Delta(H-K)$ of known low-mass stars in the EPIC field of view. The horizontal line marks the limit between stars with $(\Delta(H-K) > 0)$ and stars without a disk. The vertical line separates the stars with evidence for accretion ($\Delta(H-K) > 0$ and $EW(H_\alpha > 10$ Å) from those without.

view have considerable H_α emission since they were discovered by Schwartz (1977) in a deep red prism objective survey aiming to detect the prominent red emission line. Hence, the sample of Lupus 3 TTS described in Table 5 is most likely incomplete for WTTS that are often found in star-forming regions through X-ray observations (Neuhäuser 1997). Some of the 75 objects detected in X-rays with EPIC and that have no visible or near-infrared counterpart (see Table 6) could belong to this category [WTTS]. This bias in the study sample limits the significance of any statement on the X-ray properties's dependence on accretion or on the presence of a disk. The influence of accretion disks surrounding young PMS stars on their observed X-ray activity level is debated. Many studies found no indication that the presence of an accretion disk modifies activity levels in those stars (e.g., Lawson et al. 1996; Grosso et al. 2000; Preibisch & Zinnecker 2001, 2002; Feigelson et al. 2002; Getman et al. 2002). On the other hand, CTTS belonging to different clusters or associations are reported to be sub-luminous in the X-ray band with respect to WTTS (e.g., Neuhäuser et al. 1995; Stelzer & Neuhäuser 2001; Flaccomio et al. 2003b,c).

Figure 9 shows that some of the stars with large H_α emission have little or no IR emission above the photosphere. This is

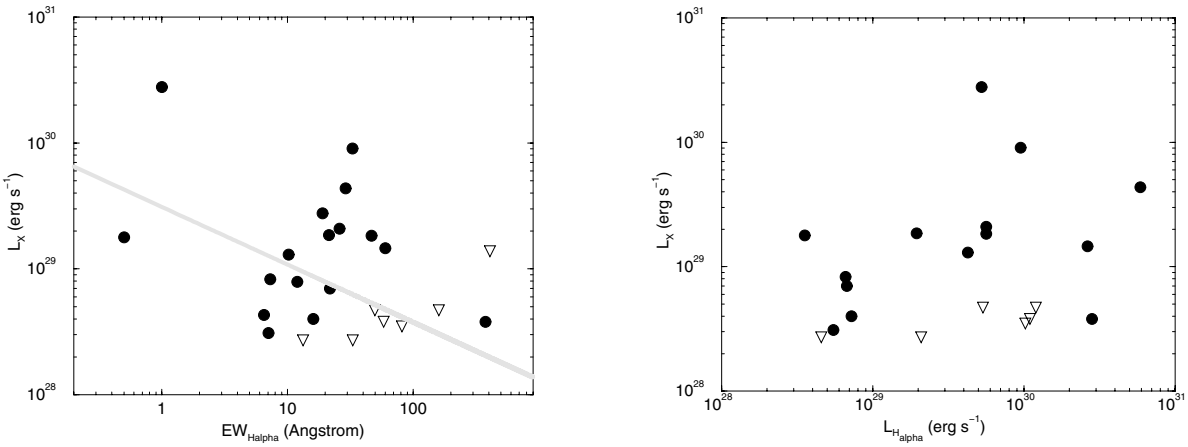

Fig. 10. X-ray luminosities vs. H_α equivalent widths (*left*) and H_α intensities (*right*). Black circles represent X-ray detections and triangles indicate upper limits of the X-ray luminosity. The thick gray line shows the EM algorithm regression fit to the $\log(L_X)$ vs. $\log(EW_{H_\alpha})$ plot computed with ASURV (see text). No correlation was found between the X-ray luminosities and the H_α intensities.

quite puzzling since accretion obviously requires the presence of a disk. One explanation is that the $\Delta(H-K)$ color excess does not discriminate well between cool low-mass stars with and without optically thick inner disks since the K-band excess traces only the hottest dust in the innermost region of the central star. Actually, many stars with circumstellar material show significant excess emission only at longer wavelengths (Haisch et al. 2001). This could explain why no correlation is found between the X-ray luminosities and the $\Delta(H-K)$ color excesses.

The Cox proportional hazard model in the ASURV software package shows the existence of a relationship between the logarithms of the H_α equivalent width (EW_{H_α}) and the X-ray luminosity. The EM linear regression (i.e., including upper limits) to the $\log(L_X)$ vs. $\log(EW_{H_\alpha})$ curve yields $\log(L_X[\mathrm{erg\ s^{-1}}]) = 29.5(\pm0.3) - 0.5(\pm0.2) \times \log(EW_{H_\alpha})$ with a standard deviation of 0.6 (see Fig. 10, left). This relation, that indicates a decreasing X-ray luminosity with increasing H_α equivalent width, supports the view that CTTS are sub-luminous in the X-ray band with respect to WTTS. The dispersion of the measurements around the best linear fit could result from non-simultaneous measurements of the X-ray luminosities and H_α equivalent widths. Damiani & Micela (1995) argued that, in the case of CTTS, the H_α equivalent width may not be a meaningful indicator since it measures the ratio between line and adjacent continuum emission that, unlike normal stars, does not arise from contiguous atmospheric layers. Indeed, CTTS H_α line profiles indicate plasma velocities greater than a 100 km s^{-1} (e.g., Mundt 1984), with signatures of winds or sometimes infalls (e.g., Hartmann & Kenyon 1990). For this reason, a quantity of more direct physical significance than the equivalent width is the actual luminosity in the line above the continuum level. The luminosity in the H_α line has been measured by Hughes et al. (1994) on a significant number of Lupus 3 stars (see Fig. 10, right). No correlation was found between the logarithms of the H_α intensity and the X-ray luminosities. For this reason and because of the sample bias towards CTTS, the present study is unable to make any conclusive statement on the X-ray property dependence of Lupus 3 stars with accretion or with the presence of disks.

4.4. X-ray luminosity vs. age

Analysis of *ROSAT* observations of young stellar clusters suggested that magnetic activity measured in the units L_X/L_{bol} increases during the first few Myr to the saturation level $\log(L_X/L_{bol}) \approx -3$ as the circumstellar disk disappears and declines on timescales of 10^7–10^8 yr in a mass dependant fashion (Flaccomio et al. 2003). This conclusion does not result from the study of the X-ray luminosity evolution within any given star-forming region, but from a comparison of several star-forming regions with different mean ages. Such a systematic behavior is not apparent for Lupus 3 stars (see Fig. 11) although statistical tests indicate a correlation between the X-ray luminosity and age of the individual stars. Some of the young TTS with age of a few Myr have an X-ray-to-bolometric-luminosity-ratio one order of magnitude below the saturation limit. On the contrary, a few objects (e.g., TTS 107 and TTS 111) with similar masses ($0.60\ M_\odot \leq M \leq 0.90\ M_\odot$), but ages over 20 Myr, are still emitting in X-rays at a significant fraction of the saturation limit. One problem in studying the X-ray luminosity vs. age dependence for any given star-forming region comes from the large uncertainties on the PMS age determination (see, e.g., Hartmann 2001). Age estimates are affected by the choice of the evolutionary tracks and the empirical determination of the bolometric luminosities and effective temperatures. Bolometric luminosities have several potential source of errors, including intrinsic photometric variability that can be very large for accreting systems, error in the estimation of extinction that can be affected by circumstellar material, and the possible presence of unresolved binary

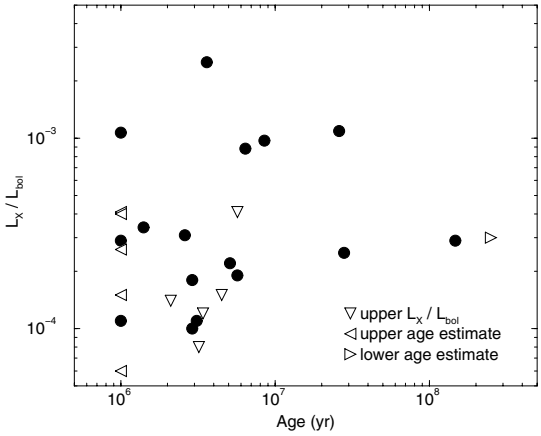

Fig. 11. X-ray luminosities vs. ages. Black circles represent X-ray detections and triangles indicate upper limits, as explained in the legend.

companions. The evolution of X-ray emission in young stars in a mass dependant fashion is an additional complication. Using mass-stratified sub-samples of PMS in the Orion Nebula Cluster, Preibisch & Feigelson (2005) found a mild decrease in X-ray luminosity over the 1–100 Myr range for ONC stars with $0.1\ M_\odot < M < 0.4\ M_\odot$ that contrasts with a faster decline for stars in the $0.5\ M_\odot < M < 1.2\ M_\odot$ mass range. In view of the limited number of stars in the present sample, a mass dependant evolution of X-ray emission cannot be investigated in the Lupus 3 region.

5. Summary

The *XMM − Newton* observation of the Lupus 3 subgroup in the Lupus dark cloud complex leads to the detection of 102 sources in the EPIC field of view, of which 96 are new X-ray detections and 77 have no visible or near-IR counterparts. The detection of this large number of new X-ray sources is an interesting result since these are candidate members of the Lupus 3 star-forming region. Their characterization will allow a better understanding of the Lupus 3 region by the determination of its initial mass function, star-forming rate, and X-ray luminosity function. The EPIC pn, MOS1, and MOS2 source list was correlated with a list of known objects, mostly pre-main sequence stars (Schwartz 1977; Krautter et al. 1997; Comeron et al. 2003), located in a 15′ radius field of view around the pointing direction. Visible and near-IR counterparts were found for 25 sources including 12 CTTSs (i.e., with an H_α equivalent width greater than 10 Å; see Table 2) and three recently discovered low-mass members. For converting the count rates of faint sources that could not be studied spectroscopically into X-ray luminosities, a 10^7 K optically thin plasma was assumed that is absorbed by a hydrogen column density derived from the visual extinction. This procedure was also used to estimate the upper limits of the X-ray luminosities of known low-mass stars in the EPIC field of view that were not detected in X-rays.

A sub-sample of 29 stars in the EPIC field of view, including 22 X-ray sources and 7 non-detections with known effective temperatures and bolometric luminosities was studied in detail. A comparison of their HR diagram positions with evolutionary models of Baraffe et al. (1998) yields estimates of their masses and ages. The study indicates that X-ray emission is detected from stars with the highest bolometric luminosities, i.e., preferably from the more massive or younger stars. The stars detected in X-rays are more X-ray active than the Sun. Their X-ray luminosities range between 3×10^{28} and 3×10^{30} erg s^{-1}. One star exceeds the saturation limit $\log(L_X/L_{bol}) \approx -3.0$ and was presumably flaring during the observation. Two young (age < 1 Myr) objects with mass estimates lower than the brown dwarf limit were detected at an X-ray luminosity level of $4–7 \times 10^{28}$ erg s^{-1}. The X-ray detected stars have X-ray surface fluxes included between 10^5 and 10^8 erg s^{-1} cm^{-2} that are comparable with the range of X-ray surface fluxes found for different structures in the solar corona. A linear correlation was found between the X-ray luminosity and the mass or the volume of the stars. Although the dependence on mass may be unexplained, a correlation with the stars' volume is qualitatively expected from some models of distributed turbulent dynamos, where the magnetic field is both generated and transported in the convection zone.

A temporal and spectral analysis was conducted on the 8 X-ray brightest sources of the sample. All these sources displayed a significant X-ray variability during the 22 ks observation. Their X-ray spectra could be fitted using an optically thin plasma emission model with two components at temperatures in the range $3–9 \times 10^6$ K and $1–50 \times 10^7$ K, respectively. Although accreting material may provide a heating mechanism for the emitting plasma, shocks heated plasma cannot attain temperatures higher than a few MK. Hot ($T > 10^7$ K) plasma components in Lupus 3 TTS may rather be caused by disruptions of magnetic fields associated with an intense flaring activity. The temperatures $T \approx 3–9 \times 10^6$ K of the "cool" plasma components are reminiscent of solar type active regions. The emission measures of the plasma components are of the order of 10^{52} cm^{-3}, in agreement with the values expected from coronal plasma in T Tauri stars, post-T Tauri stars, and active late-type dwarfs. One property of the X-ray brightest stars in Lupus 3 that is common among PMS is the low abundance of Fe. Dust continuum emission at mm wavelength from Lupus 3 TTS has been reported (Nürnberger et al. 1997) and strong H_α and CaII infrared triplet emission in the spectra of many Lupus 3 stars is interpreted as a tracer of accretion processes (Comeron et al. 2003). The low Fe abundance does not seem to be related to accretion.

Acknowledgements. I am grateful to the anonymous referee for the helpful comments that allowed me to improve the paper.

References

Alexander, D. R., Augason, G. C., & Johnson, H. R. 1991, ApJ, 345, 1014
Anders, E., & Grevesse, N. 1989, Geochim. Cosmochim. Acta, 53, 197
Arnaud, K., & Dorman, B. 2001, XSPEC User's Guide for version 11.1, http://heasarc.gsfc.nasa.gov/docs/xanadu/xspec/manual/manual.html
Argiroffi, C., Drake, J. J., Maggio, A., et al. 2004, ApJ, 609, 925
Argiroffi, C., Maggio, A., Peres, G., et al. 2005, A&A, 439, 1149
Baraffe, I., Chabrier, G., Allard, F., et al. 1998, A&A, 337, 403
Baraffe, I., Chabrier, G., Allard, F., et al. 2002, A&A, 382, 563
Briggs, K. R., & Pye, J. P. 2003, MNRAS, 345, 714
Canuto, V. M., & Mazzitelli, I. 1992, ApJ, 389, 724
Comeron, F., Fernandes, M., Baraffe, I., et al. 2003, A&A, 406, 1001
Damiani, F., & Micela, G. 1995, ApJ, 446, 341
D'Antona, E., & Mazzitelli, I. 1994, ApJS, 90, 467
den Herder, J. W., Brinkman, A. C., Kahn, S. M., et al. 2001, A&A, 365, L7
Drake, J. J., Peres, G., Orlando, S., et al. 2000, ApJ, 545, 1074
Ehle, M., Breitfellner, M., Dahlem, M., et al. 2001, The XMM−Newton Users' Handbook, http://xmm.vilspa.esa.es/user/AO2/uhb/xmm_uhb.html
Feigelson, E. D., & Nelson, P. I. 1985, ApJ, 293, 192
Feigelson, E. D., & Montmerle, T. 1999, ARA&A, 37, 363
Feigelson, E. D., Casanova, S., Montmerle, T., et al. 1993, ApJ, 416, 623
Feigelson, E. D., Broos, P., Gaffney, J., et al. 2002, ApJ, 574, 258
Feigelson, E. D., Getman, K., Grosso, N., et al. 2005, ApJS, 160, 379
Flaccomio, E., Micela, G., & Sciortino, S. 2003a, A&A, 402, 277
Flaccomio, E., Micela, G., & Sciortino, S. 2003b, A&A, 397, 611
Flaccomio, E., Damiani, F., Micela, G., et al. 2003c, ApJ, 582, 398
Fleming, T. A., Liebert, J., Giao, I. M., et al. 1988, ApJ, 331, 958
Fleming, T. A., Gioia, I. M., & Maccaro, T. 1989, ApJ, 340, 1011
Gehrels, N. 1986, ApJ, 303, 336
Getman, K. V., Feigelson, E. D., Townsley, L., et al. 2002, ApJ, 575, 354
Getman, K. V., Flaccomio, E., Broos, P. S., et al. 2005, ApJS, 160, 319
Gondoin, P. 2004a, A&A, 415, 1113
Gondoin, P. 2004b, A&A, 426, 1035
Gondoin, P., Aschenbach, B., Erd, C., et al. 2000, SPIE Proc., 4140, 1
Grosso, N., Montmerle, T., Bontemps, S., et al. 2000, A&A, 359, 113
Haisch, K. E. J., Lada, E. A., & Lada, C. J. 2001, ApJ, 553, 153
Hartmann, L. W. 2001, AJ, 121, 1030
Hartmann, L. W., & Kenyon, S. J. 1990, ApJ, 349, 190
Henize, K. G. 1954, ApJ, 119, 459
Hillenbrand, L. A., & White, R. J. 2004, ApJ, 604, 741
Houk, N., & Cowley, A. P. 1975, Michigan Catalogue of two-dimensional spectral types for the HD star, Ann Arbor: University of Michigan, Department of Astronomy, 1975
Hughes, J., Hartigan, P., & Clampitt, L. 1993, AJ, 105, 571
Hughes, J., Hartigan, P., Krautter, J., et al. 1994, AJ, 108, 1071

Imanishi, K., Koyama, K., & Tsuboi, Y. 2001a, ApJ, 557, 747
Imanishi, K., Tsujimoto, M., & Koyoma, K. 2001b, ApJ, 563, 361
Isobe, T., Feigelson, E. D., & Nelson, P. I. 1986, ApJ, 306, 490
Jansen, F., Lumb, D., Altieri, B., et al. 2001, A&A, 365, L1
Jaschek, M. 1978, CDS Inf. Bull., 15, 121
Johnson, M. 2004, Xronos User's Guide Version 5.21, http://hearsc.gsfc.nasa.gov/docs/xanadu/xronos/xronos.html
Kleinmann, S. G., Cutri, R. M., Young, E. T., et al. 1986, VizieR On-line Data Catalog: II/26
Krautter, J., Wichmann, R., Schmitt, J. H. M. M., et al. 1997, A&AS, 123, 329
Lamzin, S. A., Bisnovatyi-Kogan, G. S., Errico, L., et al. 1996, A&A, 306, 877
Lasker, B. M., Sturch, C. R., McLean, B. J., et al. 1990, AJ, 99, 2019
Lawson, W. A., Feigelson, E. D., & Huenemoerder, D. P. 1996, MNRAS, 280, 1071
LaValley, M., Isobe, T., & Feigelson, E. D. 1990, Bull. Astron. Soc. (Software Report), 22, 917
Lopez Marti, B., Eislöffel, J., & Mundt, R. 2005, A&A, 440, 139
Luhman, K. L. 1999, ApJ, 525, 466
Marino, A., Micela, G., Peres, G., et al. 2005, A&A, 430, 287
Mewe, R., Gronenschild, E. H. B., & van den Oord, G. H. J. 1985, A&A, 62, 197
Mermilliod, J.-C. 1987, A&AS, 71, 413
Mokler, F., & Stelzer, B. 2002, A&A, 391, 1025
Mukai, K. 1993, Legacy 3, 21-31
Mundt, R. 1984, ApJ, 280, 749
Nakajima, Y., Tamura, M., Oasa, Y., et al. 2000, AJ, 119, 873
Neuhäuser, R. 1997, Science, 267, 1363
Neuhäuser, R., & Comeron, F. 1998, Science, 282, 83
Neuhäuser, R., Sterzik, M. F., Schmitt, J. H. M. M., et al. 1995, A&A, 297, 391
Neuhäuser, R., Briceno, C., Comeron, F., et al. 1999, A&A, 343, 883
Nürnberger, D., Chini, R., & Zinnecker, H. 1997, A&A, 324, 1036
Ochsenbein, F., 1974, A&AS, 15, 215
Ozawa, H., Grosso, N., & Montmerle, T. 2005, A&A, 438, 661
Paresce, F. 1984, AJ, 89, 1022
Patten, B. M., & Simon, T. 1996, ApJS, 106, 489
Peres, G., Orlando, S., & Reale, F. 2004, ApJ, 612, 472
Pillitteri, I., Micela, G., Sciortino, S., et al. 2004, A&A, 421, 175
Pizzolato, N., Maggio, A., Micela, G., et al. 2003, A&A, 397, 147
Preibisch, T., & Zinnecker, H. 2001, AJ, 122, 866
Preibisch, T., & Zinnecker, H. 2002, AJ, 123, 1613
Preibisch, T., & Feigelson, E. D. 2005, ApJS, 160, 390
Preibisch, T., Kim, Y.-C., Favata, F., et al. 2005, ApJS, 160, 401
Prialnik, D., & Livio, M. 1985, MNRAS, 216, 37
Randich, S. 2000, in Stellar Clusters and Associations: Convection, Rotation, and Dynamos. Proceedings from ASP Conf., 198, ed. R. Pallavicini, G. Micela, & S. Sciortino, 401
Sanz-Forcada, J., Brickhouse, N. S., & Dupree, A. K. 2002, ApJ, 570, 799
Schmitt, J. H. M. M. 1997, A&A, 318, 215
Schwartz, R. D. 1977, ApJS, 35, 161
Stelzer, B., & Neuhäuser, R. 2001, A&A, 377, 538
Stelzer, B., & Schmitt, J. H. M. M. 2004, A&A, 418, 687
Strüder, L., Briel, U., Dennerl, K., et al. 2001, A&A, 365, L18
Swenson, J. H., Faulkner, J., Rogers, F. J., et al. 1994, ApJ, 425, 286
Tsuboi, Y., Maeda, Y., Feigelson, E. D., et al. 2003, ApJ, 587, L51
Turner, M. J. L. T., Abbey, A., Arnaud, M., et al. 2001, A&A, 365, L27
The, P.-S. 1962, Contr. Boscha Obs., 15
Vrba, F. J., & Rydgren, A. E. 1985, AJ, 90, 1490
Wichmann, R., Sterzik, M., Krautter, J., et al. 1997a, A&A, 326, 211
Wichmann, R., Krautter, J., Covino, E., et al. 1997b, A&A, 320, 185
Wuchterl, G., & Tscharnuter, W. M. 2003, A&A, 398, 1081